THERMAL ANALYSIS OF FUSED DEPOSITION

M. Atif Yardimci, Takeshi Hattori, Selcuk I. Guceri
University of Illinois at Chicago,
Chicago, Illinois USA

Stephen C. Danforth
Rutgers University
Piscataway, New Jersey USA

ABSTRACT
Fused Deposition processes involve successive melting, extrusion and solidification of thermoplastic polymer melts. Fluid mechanics and heat transfer of neat or particle-filled polymeric melts, viscoelastic deformation and solidification of the roads that are being produced, and repetitive thermal loading of the growing part are important physical processes that control the final quality of the part. Previous computational process models investigated deposition and cooling processes for single and multiple filaments. In the current study, complimentary computational models are presented for the extrusion phase of the process. Impact of liquefier and nozzle design on thermal hardware behavior and operational stability has been quantified. Also a detailed study of temperature field near the vicinity of deposition point is presented with particular emphasis on dimensional analysis and deposition of multiple material systems.

BACKGROUND

Fused Deposition process involves deposition of thermoplastic melts by a computer controlled minirobot to produce arbitrary geometry three dimensional objects (Crump, 1992.) Fabricated objects possess a two level hierarchical meso-structure, which consists of curvilinear roads packed into discrete layers. The thermal energy stored in the molten material is redistributed into the part through conduction, and is consumed by lateral convection cooling. The redistribution of thermal energy ensures bonding at the interfaces of deposited roads, and generates the structural integrity of the part. Material delivery into the workvolume can be achieved by a liquefier which employs a self-extruding filament (Comb et.al, 1994), a fluid metering rotary pump (Batchelder et.al, 1994) or through a high-pressure plunger system (Hilmas, 1996). The road cross-sections are shaped through fountain flow of polymer melt between the previously deposited material and nozzle tip, resulting in flattened ellipsoids. These ellipsoid shapes are basically rectangles with two semi-circles attached at each lateral side of the road, which have the layer thickness as their diameter Recently computer controlled surface forming mechanisms, trowels, have been proposed to shape the road cross-sectional geometries (Khoshnevis, 1997). The available material set for filament deposition techniques has been increased through introduction of particles into the feed-stock, which enabled the production of intermediate powder processing products, particulate polymeric composites or *green* bodies, that can be processed further to obtain porous and/or fully dense metallic and ceramic articles (Geiger, 1994), (Agarwala et.al, 1995).

Previous process modeling effort for Fused Deposition was concentrated on the cooling behavior of single and multiple filaments (Yardimci et.al, 1995), (Yardimci and Guceri, 1996),

and development of build file, *SML* file, interpretation and analysis tools for heuristic simulation of part building with FD (Yardimci et.al, 1996). In the current work four critical aspects of extrusion process are addressed: thermal design of liquefier entrance, analysis of melt front location in the liquefier, degree of cooling in the nozzle and the impact of nozzle design on operational stability of the hardware. Also a deposition level thermal model is presented to investigate the effects of relevant non-dimensional numbers, Peclet and Biot numbers, on temperature distribution across multiple filament configurations.

LIQUEFIER DESIGN

The operation of the liquefier is controlled through two different channels: whereas flow control is facilitated through servo controllers that command the motion of the traction rollers; temperature regulators adjust heater power to keep liquefier temperature at the constant pre-set value. The decoupled nature of the temperature regulation from motion or flow control generates unique challenges for liquefier design, e.g. the temperature at the liquefier entrance shall not exceed a critical value even though the liquefier temperature is constant at pre-set temperature, the liquefier length should be long enough to achieve the desired temperature at its end for all flowrate conditions.

Entrance Insulation

In the current section the conduction heat transfer phenomena at liquefier entrance, Figure 1, is analyzed. A thermal model is presented for the prediction of entrance temperatures with different liquefier designs (geometry of filament / liquefier / seperator plate), material properties (thermal conductivity of filament and plate) and processing conditions (degree of convective cooling at the entrance). The axisymmetric conduction equation can be written for a heterogeneous domain as:

$$\frac{1}{r}\frac{\partial}{\partial r}\left(k\,r\,\frac{\partial T}{\partial r}\right)+\frac{\partial}{\partial z}\left(k\,\frac{\partial T}{\partial z}\right)=0$$

$$-k\frac{\partial T}{\partial n}=h_1\left(T-T_1\right)\ @\ \vec{r}\in\Gamma_1\quad;\quad -k\frac{\partial T}{\partial n}=h_2\left(T-T_2\right)\ @\ \vec{r}\in\Gamma_2 \tag{1}$$

$$T=T_0\ @\ \vec{r}\in\Gamma_3\ ,\ \frac{\partial T}{\partial n}=0\ @\ \vec{r}\in\Gamma_4$$

, where r and z are radial and axial coordinates, k is spatially distributed thermal conductivity, T_0 is liquefier temperature, h_1 and T_1 are liquefier side convective cooling coefficient and temperature and h_2 and T_2 are entrance side convective cooling coefficient and temperature respectively. Finite volume method is employed in the numerical discretization of the governing equations on a triple block grid. The resulting set of equations are solved using a pseudo-transient scheme, Alternating Direction Implicit (ADI). A sample solution for k_f = 0.2 W/(m K), k_p = 3.0 W/(m K), k_l = 400.0 W/(m K), h_1 = 100 W/(m^2 K), h_2 = 10 W/(m^2 K), T_0= 270°C, T_1= 20°C, T_2= 70°C, w_p= 2mm, l_1= 10 mm, l_2= 20 mm, r_f= 0.914 mm, r_{liq}= 10 mm, is presented in Figure 2.a. The sharp drop in temperature through the seperator plate is remarkable, hence the width of the seperator plate can be effectively utilized as a design variable. The dimensional

analysis of governing equation and boundary conditions reveals that plate and filament Biot numbers can consolidate the number of process variables.

$$\theta = \frac{T_e - T_2}{T_0 - T_2} \quad , \quad Bi_p = \frac{h_2\ w_p}{k_p} \quad , \quad Bi_f = \frac{h_2\ 2r_f}{k_f} \tag{2}$$

Furthermore, through definition of non-dimensional entrance temperature the operation map of the liquefier has been estimated with ten numerical experiments documented in Figure 2.b. Entrance temperature decrease with increasing plate and filament Biot numbers and safe liquefier designs can be predicted using the generated map for different filament materials.

Location of Melt Front

The heating of the filament inside the liquefier is governed by the two-dimensional axissymetric steady-state advection-conduction equation (Burmeister, 1983). A resistive heater is wrapped around the aluminum liquefier. Due to high thermal conductivity of this material, temperature is more or less homogeneous along the tube. Hence it becomes appropriate to replace constant heat flux wall boundary condition with constant wall temperature. Furthermore since the filament remains solid upto the point of melting, the flow may be approximated with plug flow, i.e. constant flow across the cross-section. The solution of this Graetz problem in non-dimensional form is:

$$\theta = 2\sum_{n=1}^{\infty} e^{\left(-\lambda_n^2 z'\right)} \frac{J_0\left(\lambda_n r'\right)}{\lambda_n J_1\left(\lambda_n\right)} \quad , \quad J_0\left(\lambda_n\right) = 0 \quad , \quad \theta = \frac{T - T_0}{T_2 - T_0}$$
$$r' = \frac{r}{r_f} \quad , \quad z' = \frac{\alpha}{V r_f} \frac{z}{r_f} \tag{3}$$

, where r' and z' are non-dimensional coordinates, V is filament velocity, α is thermal diffusivity, λ_n are roots of zero order Bessel function of first kind, J_0, and J_1 is first order Bessel function of first kind. If a melting temperature, T_m, is defined for the material; the melt front location, z'_m i.e. the axial location at which the temperature at the center of the filament reaches T_m, can be calculated from:

$$\theta_m = 2\sum_{n=1}^{\infty} \frac{e^{\left(-\lambda_n^2 z'_m\right)}}{\lambda_n J_1\left(\lambda_n\right)} \tag{4}$$

Examination of definition of z' reveals that the actual melt front distance is linearly proportional to filament speed and square of filament diameter and inversely proportional to material diffusivity.

Degree of Cooling in the Tip

The liquefier temperatures set on the front panel of Fused Deposition equipment may not reflect the correct deposition temperature, since the deposition tip itself is not heated and insulated. Axissymmetric heat conduction equation has been solved for nozzle geometry presented in Figure 3.a (representing a T16 nozzle), using linear triangular ring finite elements,

to investigate the degree of cooling in the nozzle. The base of the nozzle is kept at liquefier temperature, 270 °C for the cases presented in the report; external surface of the nozzle is insulated half way down, which represents the band heater around the threaded section in Fused Deposition hardware, and the rest of the external surface is open to convective cooling, with a convection coefficient of h = 100 W/(m^2 K) and an envelope temperature of 70 °C. The internal surface of the nozzle which interfaces the filament has been simulated using an adiabatic boundary condition. This boundary condition represents the worst case scenario, minimum tip temperature, since during deposition there will be net heat transfer from filament to the nozzle. A sparse linear solver has been utilized for the solution of resulting set of equations. Two materials were considered aluminum (k = 400 W/(m K)), and stainless steel (k = 100 W/(m K)). The resulting temperature distributions are shown in Figures 3.a and 3.b. Higher thermal conductivity material resulted in higher tip temperatures, although total heat loss was higher. Both materials resulted in tip to base temperature differentials which were within %6 of the base to envelope temperature differential. A new tip design with a metal core and insulating coating may be the best choice to keep liquefier to tip temperature differential at a minimum.

Impact of Nozzle Design on Liquefier Requirements

The internal transition angle of the nozzle from the filament diameter to extrusion tip diameter is generally 120°, the tip angle of the drill Such large contraction angles combined with large contraction ratios of 6:1 may result in the formation of corner vortices (also named dead zones in extrusion practice) (Liang et.al, 1996). The presence of these vortical regions is especially critical for particle loaded materials, since the regions may create flow instabilities and eventual clogging of the nozzle. One remedy is to decrease the transition angle below the Natural Convergence Angle (NCA) below which vortical regions disappear. However lower transition angles result higher cumulative shear stresses and pressure drops, since the effective Reynolds number of the flow is much less than one for polymer melts through capillaries. Higher pressure drops in turn may impede the operational stability of the hardware causing filament buckling.

The pressure drop of neat or particulate loaded thermoplastic melts, described with shear thinning power law fluid behavior, across circular straight channels may be found in literature (Michaeli, 1992). The pressure loss in a conical convergent tube may be represented as the sum of discrete pressure losses of equivalent infinitesimal tubes connected in series and contract in diameter as:

$$\tau = \left(\frac{\dot{\gamma}}{\phi}\right)^{1/m} \quad , \quad \Delta p = \left[\frac{(m+3)(2L)^m \dot{Q}}{\pi R^{m+3} \phi}\right] \quad \textit{Tubes}$$

$$\Delta p = \frac{mL}{3(R_0 - R_1)}\left[\frac{(m+3)2^m \dot{Q}}{\pi \phi}\left(\left(\frac{1}{R_1}\right)^3 - \left(\frac{1}{R_0}\right)^3\right)\right]^{1/m} \quad \textit{Cone Sections} \qquad (5)$$

The Euler buckling analysis of the filaments results in the following expression for critical pressure drop:

$$P_{cr} = \frac{\pi^2 \, E \, d_f^2}{16 \, L_f^2} \tag{6}$$

Combining equations 5 and 6 with the empirical data on NCA for RU955 material, the operation windows have been predicted for T15 and T25 tips under different internal cone angles, as shown in Figure 4 a. & b. The filament elastic modulus was selected as E = 15MPa, and filament buckling length as 7.62 mm (0.3"). It is apparent that there is a upper limit on flow rates for given filament and tip diameters, and material properties.

DETAILED DEPOSITION MODEL

The temperature field near the vicinity of deposition region can be analyzed in detail, if one would assume: a. the previously deposited material had ample time to cool down an equilibrium temperature, b. temperature field can be averaged across the thickness reducing the dimensionality of the problem by one, c. the heat transfer to ambient and previous layer can be modeled effectively with heat sink terms. The resulting quasi-steady state, two dimensional modified advection conduction equation in the reference frame of the moving deposition head may be written as:

$$\rho \, c_p \, V \frac{\partial T}{\partial x} = \frac{\partial}{\partial x}\left(k \frac{\partial T}{\partial x}\right) + \frac{\partial}{\partial y}\left(k \frac{\partial T}{\partial y}\right) - \frac{h_\infty}{th}\left(T - T_\infty\right) - U\left(T - T_{sub}\right)$$

$$T = T_0 \, , @ \, \vec{r} \in \Gamma_1 \quad , \quad T = T_{sub} \, , @ \, \vec{r} \in \Gamma_2 \tag{7}$$

$$-k \frac{\partial T}{\partial n} = \frac{h_\infty}{th}\left(T - T_\infty\right) , @ \, \vec{r} \in \Gamma_3 \quad , \quad \frac{\partial T}{\partial n} = 0 \, , @ \, \vec{r} \in \Gamma_4$$

, where h_∞ is envelope convective cooling coefficient, T_∞ is envelope temperature, T_{sub} is equilibrium temperature of previously deposited material, U is a general heat transfer coefficient which may be defined as the ratio of effective interface thermal conductivity to a characteristic depth at which equilibrium temperature is reached in previous layer, and th is road thickness. It should be noted the conservative definition of diffusive heat flux terms enables the equation to be applicable to heterogeneous material systems.

The governing equation is discretized with finite volume method on multiple-block grids, Figure 5. ADI method is utilized for the solution of discrete equations utilizing a pseudo time integration scheme.

Dimensional Analysis

The governing equation may be non-dimensionalized as:

$$x' = \frac{x}{w} \quad , \quad y' = \frac{y}{w} \quad , \quad \theta = \frac{T - T_\infty}{T_0 - T_\infty}$$

$$Pe_w \frac{\partial \theta}{\partial x'} = \frac{\partial}{\partial x'}\left(\frac{\partial \theta}{\partial x'}\right) + \frac{\partial}{\partial y'}\left(\frac{\partial \theta}{\partial y'}\right) - Bi_w \frac{w}{th}\theta - Uw^2\left(\theta - \theta_{sub}\right) \tag{8}$$

$$\theta = 1 \,, @\vec{r} \in \Gamma_1 \quad ; \quad \theta = \theta_{sub} \,, @\vec{r} \in \Gamma_2$$

$$-\frac{\partial \theta}{\partial n} = Bi_w \frac{w}{th}\theta, @\vec{r} \in \Gamma_3 \quad , \quad \frac{\partial \theta}{\partial n} = 0 \; @\vec{r} \in \Gamma_4$$

,where

$$Pe_w = \frac{\rho c_p V w}{k} \quad , \quad Bi_w = \frac{h_\infty w}{k} \tag{9}$$

Six numerical experiments have been conducted to investigate effect of Peclet and Biot numbers on temperature distributions, by assuming θ_{sub}=0 and U = 0. The results are shown in Figures 6 and 7. Peclet number variations mainly effected the axial, along deposition direction, temperature distributions. Higher Peclet configurations result in longer 'active interface lengths', and hence better interface bonding for the production of same geometrical features. However the cooling time of road-substrate interface has been found to be weakly dependent on Peclet number due to linear inter dependence of Pe, V and time. Biot number variations on the other hand produced a more isotropic effect on the temperature distributions, with high Biot numbers resulting in shorter 'active interface lengths' and shallower extent of the heat affected zone in lateral direction. Since deposition velocity does not appear in Biot number definition, the reductions in active lengths also corresponded to reductions in residence times.

Multiple Materials

Fabrication of spatially distributed materials, embedded structures and topologically optimized composite articles require sequential deposition of neat and particle filled materials in Fused Deposition. Thermal behavior of parts composed of multiple materials may be different during production, due to differences in their thermal properties. Additional parameters that would characterize the deposition sequence are needed to investigate different thermal behavior patterns during deposition. As an example the sequential production of a three road part made out of two different material systems is considered. Thermal conductivities of 'plastic'(P) and 'metal filled'(M) phase are k = 0.2 W/(m K) and 3.0 W/(m K) respectively. Following parameters were considered for both of the materials in the current study: ρ=1200 kg/m^3, c_p=1500 J/(kg K), V = 20 mm/s, th = 0.25 mm, w = 0.5 mm, T_0 = 270°C, h_∞=100 W/(m K), T_∞=70°C. Two stacking sequences were considered, P/M/M and M/M/P. The results are depicted in Figure 8 a & b. For first stacking sequence the lateral penetration of heat effected zone is limited compared to the second sequence, however the active interface length is longer due to smaller road 1 Peclet number.

CONCLUSIONS

A set of computational tools has been presented for the analysis of extrusion phase in Fused Deposition. Design methodologies have been developed for liquefier entrance, liquefier length, unheated tip and internal duct design through employment of analytical and

computational thermal design tools. Particular emphasis has been placed on identification of non-dimensional groups to consolidate number of variables in the analysis.

Also a detailed description of quasi-steady state, two dimensional deposition thermal model is presented. Finite volume method on non-uniform multi-block grids has been utilized in the formulation. Peclet and Biot numbers based on road width were identified as important parameters from dimensional analysis, and their effect on temperature distributions is demonstrated through computational experiments. Peclet number has been found to modify the temperature field anisotropically (dominantly in axial direction) whereas Biot number changed temperature distributions isotropically. Also building scenario effects have been investigated for a two material, three road configuration. Significant penetration depth were observed.

REFERENCES

1. Agarwala M. K., van Weeren R., Vaidyanathan R., Bandyopadhyay A., Carrasquillo G., Jamalabad V., Langrana N., Safari A., Garofalini S. H., Danforth S. C., Burlew J., Donaldson R., Whalen P., Ballard C., "Structural Ceramics by Fused Deposition of Ceramics," *Proceedings of SFF Symposium 1995*, pp. 42-49, 1995.
2. Batchelder J. S., Curtis H. W., Goodman D. S., Gracer F., Jackson; R. R., Koppelman G. M., Mackay J. D., *Model generation system having closed-loop extrusion nozzle positioning*, US Patent #5,303,141; April 12 1994.
3. Burmeister, L. C., *Convective Heat Transfer*, pp. 218, John Wiley & Sons, 1983
4. Crump S., *Apparatus and method for creating three-dimensional objects,* US Patent #5,121,329, June 9, 1992.
5. Comb J. W., Priedeman W. R., Turley P. W., "FDM technology process improvements," *Proceedings of SFF Symposium 1994*, pp. 42-49, 1994.
6. Geiger M., Steger W., Greul M., Sindel M., "Multiphase Jet Solidification - a new process towards metal prototypes and a new data interface," *Proceedings of SFF Symposium 1994*, pp. 9-16, 1994.
7. Hilmas G. E., Lombardi J.L., Stuffle K., "Recent developments in extrusion freeform fabrication (EFF) utilizing non-aqueous gel casting formulation," *Proceedings of SFF Symposium 1996*, pp. 432-439, 1996.
8. Khoshnevis B., "Contour Crafting: A new Rapid Prototyping process," *Proceedings of The Seventh International Conference on Rapid Prototyping*, March 31-April 3 1997, pp. 13-22, 1997.
9. Liang J.Z., Ling Y. Z., Li. R.K.Y., Tjong S.C., "Quantitative description of vortical region length of non-newtonian fluids through an abrupt contraction," *ASME - AMD vol.217*, pp. 105-107, 1996.
10. Michaeli W., *Extrusion Dies for Plastics and Rubber: Design and Engineering Computations*, 2nd Edition, Hanser Publishers, 1992.
11. Yardimci M. A., Guceri S.I., Danforth S. C, Safari A., "Numerical modeling of Fused Deposition processing", *Proceedings of The ASME Materials Division, MD-Vol. 69-2*, pp. 1225-1236, 1995
12. Yardimci M. A., Guceri S. I., "Conceptual framework for the thermal process modeling of Fused Deposition", *Rapid Prototyping Journal*, vol.2, no.2, pp. 26-31, 1996

13. Yardimci M. A., Guceri S. I., Agarwala M., Danforth S. C., "Part quality prediction tools for Fused Deposition processing," *Proceedings of SFF Symposium 1996*, pp. 539-548, 1996.

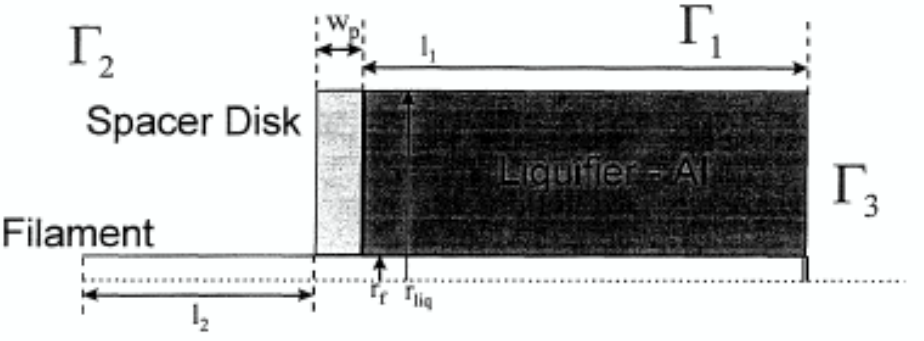

Figure 1. Liquefier Entrance

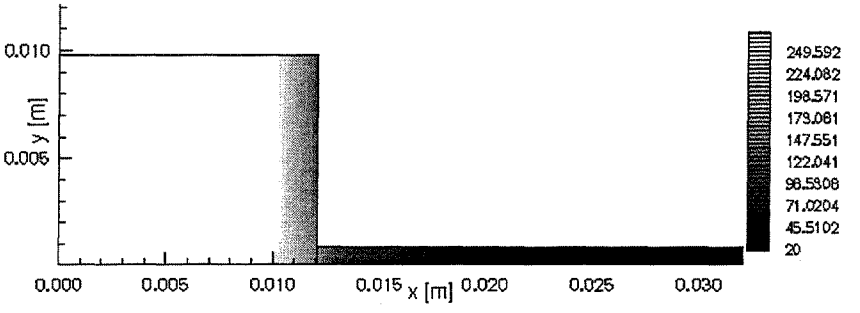

a.

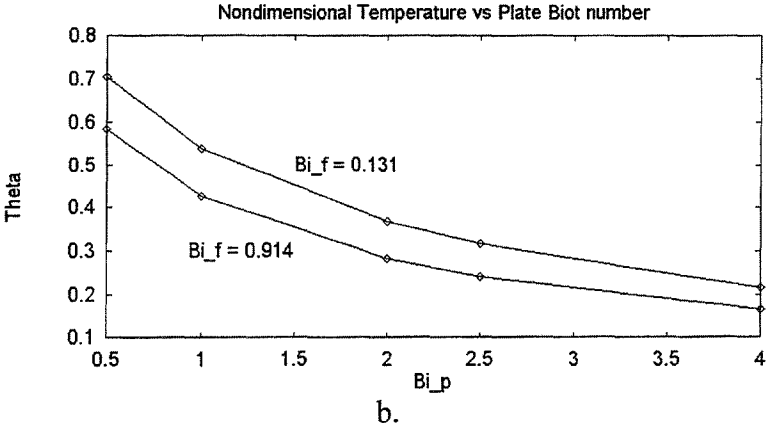

b.

Figure 2. a. Temperature distribution at liquefier entrance for example case, b. Dependence of entrance temperature on plate and filament Biot numbers

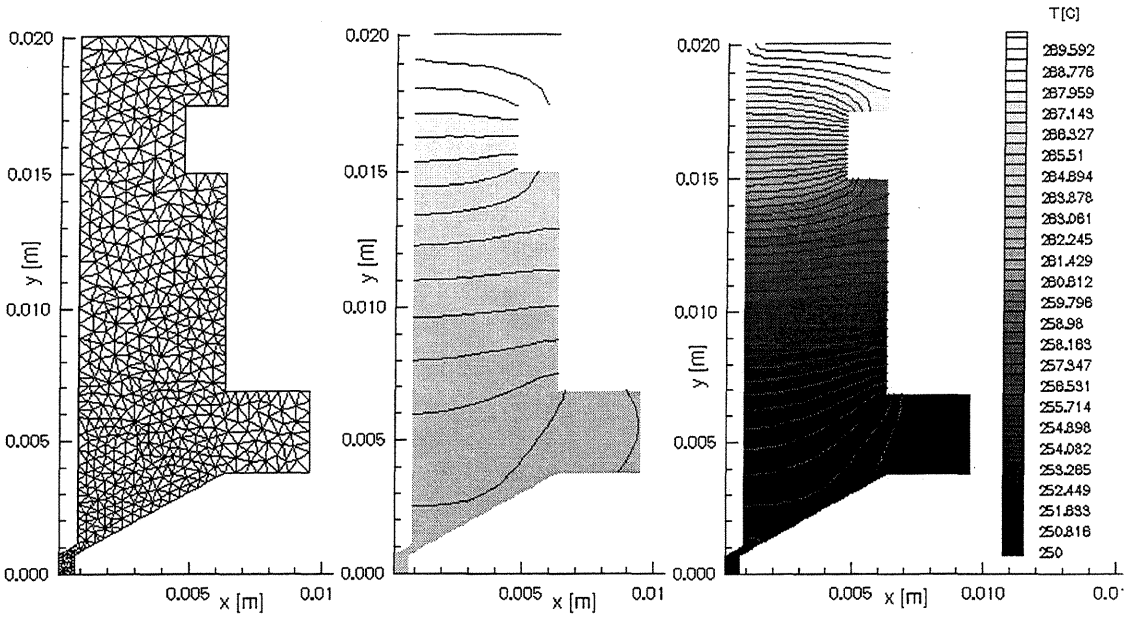

a. b. c.

Figure 3. FE Mesh (a) and Temperature distributions for Aluminum (b) and Steel (c) T16 (0.0016" diameter) nozzles

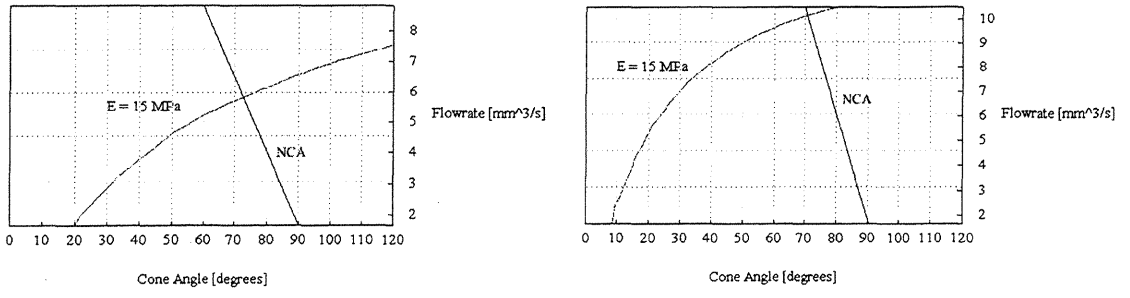

a. b

Figure 4. Operation windows of RU955 with T15 (a) and T25 (b) nozzles

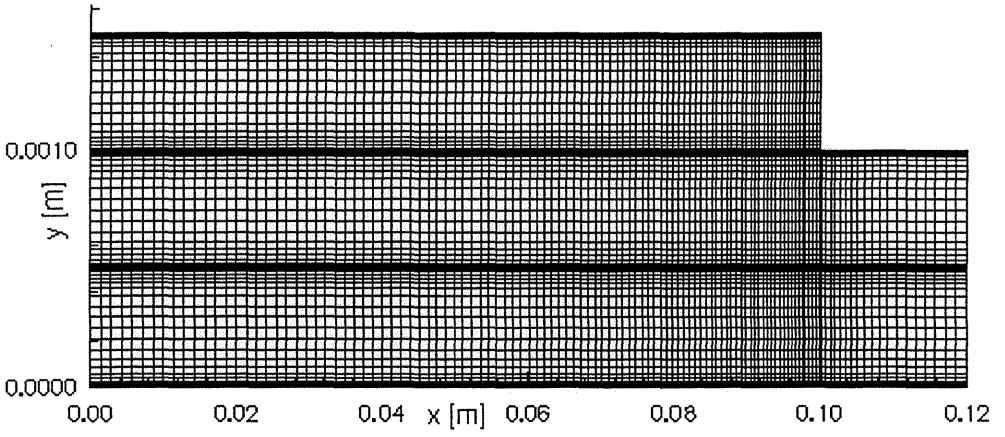

Figure 5. Employed multi-block grid for quasi steady state deposition model

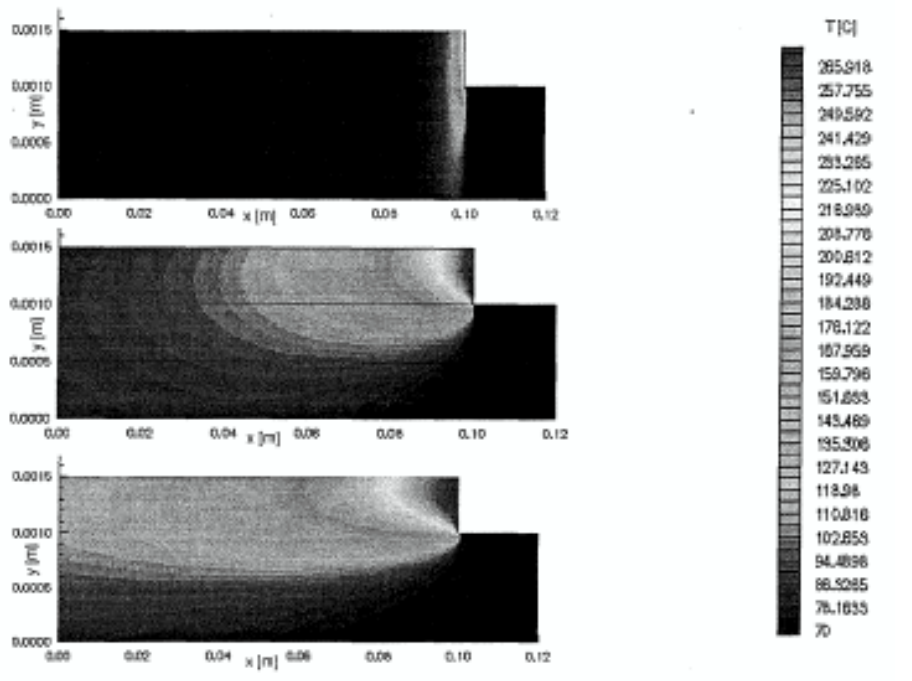

Figure 6. Effect of Peclet number variations on temperature distributions, Bi_w w/th = 0.5; a. Pe_w = 5.0, b. Pe_w = 90.0, c. Pe_w = 180.0

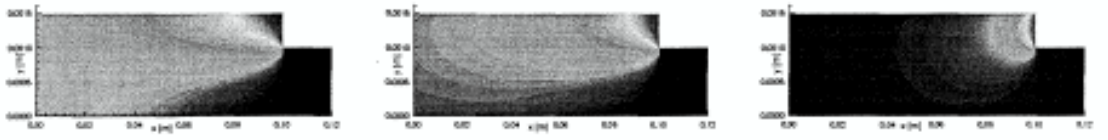

a. b .c.

Figure 7. Effect of Biot number variations on temperature distributions, Pe_w = 90.0, w/th=2.0; a. Bi_w = 0.0125, b. Bi_w = 0.125, c. Bi_w = 1.0

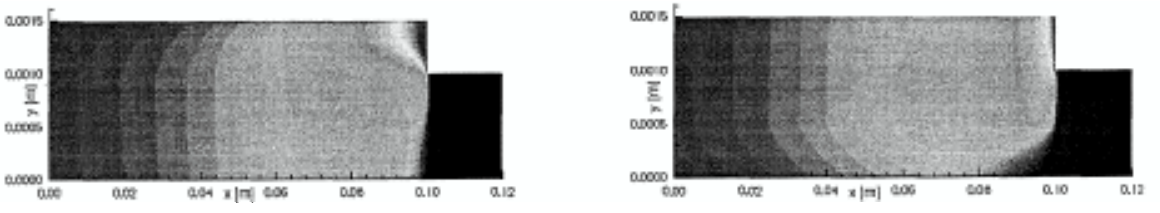

a. b.

Figure 8. Multiple Material Fused Deposition, a. Plastic/Metal/Metal, b. Metal/Metal/Plastic